IOPscience iopscience.iop.org

Home Search Collections Journals About Contact us My IOPscience

Band alignment and conversion efficiency in Si/Ge type-II quantum dot intermediate band solar cells

This content has been downloaded from IOPscience. Please scroll down to see the full text.

2007 Nanotechnology 18 405401

(http://iopscience.iop.org/0957-4484/18/40/405401)

View the table of contents for this issue, or go to the journal homepage for more

Download details:

IP Address: 140.113.38.11

This content was downloaded on 26/04/2014 at 03:52

Please note that terms and conditions apply.

Nanotechnology **18** (2007) 405401 (12pp) doi:10.1088/0957-4484/18/40/405401

Band alignment and conversion efficiency in Si/Ge type-II quantum dot intermediate band solar cells

A M Kechiantz[1,2,4], L M Kocharyan[3] and H M Kechiyants[1]

[1] Department of Applied Chemistry and Institute of Molecular Science, National Chiao Tung University, Hsinchu, Taiwan
[2] Scientific Research Division, State Engineering University of Armenia, Yerevan, Armenia
[3] Department of Physics, Yerevan State University, Yerevan, Armenia

E-mail: arakech@mail.nctu.edu.tw

Received 6 April 2007, in final form 1 August 2007
Published 11 September 2007
Online at stacks.iop.org/Nano/18/405401

Abstract
The concept of the intermediate band (IB) solar cells (SC) offers the promise of achieving 63% conversion efficiency devices. The effect of the type II band alignment in the quantum dot (QD) IB SCs on the above percentage is analyzed and the potential of the Ge/Si system for fabrication of the type II QD IB SC is discussed. Also, it is shown that the increase of the sunlight concentration leads to the rise of the potential barrier around QDs and the concentration of $S_x \approx 700$ can induce the $\varepsilon_L = 0.2$ eV height barrier in the Ge/Si system, making this a significant result. Furthermore, the increase of the sunlight concentration leads to the separation of the quasi-Fermi levels from the confined states and also leads to the decrease of the recombination activity in QDs. The two-photon absorption in QDs increases rapidly and dominates over recombination at the moderate concentration. As the contributions of QDs to both the photo- and dark currents in the type II QD IB SC are evaluated it is shown that, compared to the conventional Si SCs, the type II Ge QD IB Si SCs can generate about 25% higher photocurrent and conversion efficiency.

(Some figures in this article are in colour only in the electronic version)

List of symbols

α_C and α_V — The absorption coefficient for the direct electron transitions from the confined state into the conduction band and from the valence band into the confined state within the Ge QDs, $\alpha_C = \beta_C(N_D\vartheta - p_D)$ and $\alpha_V = \beta_V p_D$, $\alpha_C = \alpha_V \approx 2.4 \times 10^3$ cm^{-1}

α_Γ — The absorption coefficient for the direct electron transitions in the bulk Ge, $\alpha_\Gamma \approx \beta_\Gamma N_{C\Gamma}$, $\alpha_\Gamma \geqslant 5 \times 10^3$ cm^{-1}

ϑ — The number of confined states per QD involved in the absorption, $\vartheta = 10$

β_C, β_V and β_Γ — The relevant absorption cross sections, $\vartheta\beta_C \approx 8 \times 10^{-13}$ cm^2 [21], $\vartheta\beta_V = 2 \times 10^{-13}$ cm^2 [20], $\beta_\Gamma \approx 2.5 \times 10^{-14}$ cm^2, $\vartheta = 10$, $\beta_C = 3 \times 10^{-14}$ cm^2 and $\beta_V = 2 \times 10^{-14}$ cm^2 are a realistic approximation

C_A — The Auger coefficient, $C_A = 10^{-31}$ cm^6 s^{-1} [17]

D_V — The in-plane diffusion coefficient of holes within the $Si_{1-x}Ge_x$ layer, $D_V = 10$ cm^2 s^{-1}

d — The thickness of the n-doped multilayer absorber

e, r and er — The electronic charge, the electron space

[4] Permanent e-mail: MRS_Armenia@yahoo.com

 © 2007 IOP Publishing Ltd Printed in the UK

	coordinate, and the electric dipole, respectively
ε_J	The potential barrier for the dark current in the depletion layer of the ideal p–n junction
ε_{Si} and ε_{Ge}	Indirect fundamental bandgap of the strained Ge and Si, $\varepsilon_{Si} = 1.12$ eV
ε_1 and ε_2	The offsets in the conduction and valence bands at the heterojunction between the Si and $Si_{1-x}Ge_x$ layers
ε_{SG}	Bandgap of the $Si_{1-x}Ge_x$ layer of the spacer, $\varepsilon_2 = \varepsilon_{Si} - \varepsilon_{SG}$
ε_L	The illumination-induced barrier around the Ge QD, $\varepsilon_L = e^2 p_D/\varepsilon R N_D$
ε	The dielectric constant of the Si spacer, $\varepsilon = 11.9$
R	The height of the Ge QDs, $R \approx 3$ nm [26]
ε_Γ and ε_V	The bandgaps between the confined state and the Γ valley in the conduction band, and between the confined state and the Γ valley in the valence continuum band, $\varepsilon_\Gamma = 0.87$ eV [40], $\varepsilon_V = 0.43$ eV
g_C, g_V, g_{Si} and g_Γ	The integral intensities of infrared photons in the $\varepsilon_V < \hbar\omega < \varepsilon_\Gamma + \varepsilon_V$, $\varepsilon_V < \hbar\omega < \varepsilon_\Gamma$, $\varepsilon_{Si} < \hbar\omega$ and $\varepsilon_\Gamma + \varepsilon_V < \hbar\omega$ regions of the solar spectrum, $g_C = g_V = 1.05 \times 10^{17}$ cm^{-2} s^{-1}, $g_{Si} = 2.37 \times 10^{17}$ cm^{-2}s^{-1} and $g_\Gamma = 1.95 \times 10^{17}$ cm^{-2}s^{-1} [36];
G	The intensity of the net electron transitions from the valence band into the conduction band via the confined electronic state in the QDs
j_C and j_V	The intensity of irradiation-induced transitions from the confined electronic state into the conduction band and from the valence band into the confined electronic state in the QDs
j_{RC} and j_{RV}	The increase in the intensity of recombination per QD from the conduction band into the confined state, and from the confined state into the valence continuum band
j	The total photocurrent generated in the Ge QD buried Si solar cell, $j \approx 47.5$ A cm^{-2} at the concentration of $S_X \approx 1000$
j_{Si}	The total photocurrent generated in the conventional Si solar cells, $j_{Si} \approx 38$ A cm^{-2} [36] at the concentration of $S_X \approx 1000$
L	The distance between buried contacts shown in figure 2, $L = 10$ μm
L	The symmetry point of the Brillouin zone
Γ	The symmetry point in the center of the Brillouin zone
Δ	The symmetry line of the Brillouin zone
$\Delta2$ and $\Delta4$	The valleys on the Δ symmetry line of the Brillouin zone in the conduction band
m_Γ	The electron mass in the Γ valley in the conduction band of the bulk Ge, $m_\Gamma = 0.041$ m_o [40]
n	The ideality factor of the p–n junctions
N_D	The volume density of the Ge QDs, $N_D = 2 \times 10^{16}$ cm^{-3} [26]
$N_{C\Gamma}$	The effective number of oscillators involved in the direct transitions in bulk Ge, $N_{C\Gamma} = 2 \times 10^{17}$ cm^{-3} [40]
N_V	The density of electronic states in the valence band of the $Si_{1-x}Ge_x$ layer, $N_V \approx 2N_{DV}$
N_{DV}	The density of states in the valence continuum band of the Ge QDs
Ω	The volume of the Ge QD, $\Omega = 10^3$ nm^3 [22, 26]
p_D	The volume density of confined holes
p_V	The density of holes within the $Si_{1-x}Ge_x$ layer of the n-doped Si/$Si_{1-x}Ge_x$/Si spacer (including photo-generated holes), $p_V \approx \alpha_V(g_V + g_\Gamma)S_X(L^2/D_V)/[1 + (\Omega N_D N_{DV} L^2/\tau_V D_V N_V)\exp(-\varepsilon_L/kT)]$
S_X	The concentration of sunlight, $S_X = 10^3$
V_{OC}	The open-circuit voltage induced in the Ge QD buried Si solar cell
V_{OCSi}	The open-circuit voltage induced in the conventional Si solar cells
η	The conversion efficiency of the Ge QD buried Si solar cell
η_{Si}	The conversion efficiency of the conventional Si solar cells, $\eta_{Si} = 37\%$ [36]
τ_C	The inter-band recombination lifetime that includes all radiative and nonradiative (and interface) mechanisms for the electron transitions from the conduction band of the Si/$Si_{1-x}Ge_x$/Si spacer into the confined state in the QD, $\tau_C = 1$ μs in the type-II Ge QDs buried in the Si matrix [14], $\tau_C = 1$ μs in the type-II GaSb QDs buried in the GaAs matrix [15]
τ_V	The intra-band relaxation lifetime that includes both radiative and nonradiative mechanisms for the electron transitions from the confined state into the valence continuum band in the Ge QD, $\tau_V = 50$ ps for the intra-band relaxation lifetime [16]
τ_A	The Auger recombination lifetime given by $\tau_A = 1/C_A p_V^2$
z	The distance from the front-side surface

ε_{Δ}	The energy gap for the direct optical transitions within the Si/$Si_{1-x}Ge_x$/Si spacer, from the Δ valence band ($E_{V\Delta}$) into the Δ conduction band ($E_{C\Delta}$), $\varepsilon_{\Delta} = E_{C\Delta} - E_{V\Delta}$
E_{Γ} and E_{Δ}	The energies of the Γ and Δ bands in the conduction and valence bands
$E_{\Delta 2}$ and $E_{\Delta 4}$	The energies of the split Δ bands in the conduction band
lh and hh	The light and heavy holes

1. Introduction

The concept of intermediate band (IB) solar cells (SC) has attracted much attention in the last decade. This concept aims to bring about higher conversion efficiency devices than the multi-junction SCs [1]. Like the conventional solar cells, IB SCs exploit one-photon absorption for generating the photocurrent. However, these SCs also exploit the two-consecutive-photon-induced electron transitions via the intermediate states for generating an extra photocurrent [1]. In fact, the IB SC concept exploits nonlinearity in the absorption and therefore the concept will gain from the concentration of sunlight. The compatibility with the high concentrator technology gives IB SCs an additional advantage for reducing electricity costs due to the substitution of expensive semiconductor cells with low-cost optics [2].

In the past decade, considerable insight into the optical and photoelectrical features of IB SCs has been achieved [3–9]. Recently the IB SCs have been fabricated from InAs QDs sandwiched between n- and p-doped GaAs layers and their operation demonstrated [10, 11]. However, the induced photovoltage was lower than in the control GaAs SC. A possible explanation of the low photovoltage is the thermal generation of carriers in InAs QDs. These carriers can escape from the QDs embedded in the build-in electric field [12] producing an extra dark current that may reduce the separation of the quasi-Fermi levels and suppress the photovoltage. It seems that the InAs/GaAs system may not be the best material choice for IB SCs [10, 11].

The separation of quasi-Fermi levels is a paramount problem for the energy conversion in IB SCs [3–5]. The QD confined states in IB SCs are like the electronic states of impurity centers. The states easily convert into fast recombination centers and come into equilibrium either with the conduction band or with the valence band. For example, impurity centers embedded in GalnNAs solar cells arrest the quasi-Fermi level, increase the recombination and impact the photovoltage in the cells [13]. However, the recombination at QDs also depends on the potential barriers around QDs. The recombination is reduced when the potential barrier separates the electrons and the holes in a real space. For instance, the inter-band recombination in the type-II GaSb QDs buried in GaAs and in the type-II Ge QDs buried in Si is extended to 1 μs, due to the potential barrier in the conduction band [14, 15]. Another feature of the type-II QDs is the irradiation-induced potential barrier around QDs [16]. The higher the sunlight concentration, the higher is the barrier induced. Despite its importance for the operation of IB SCs

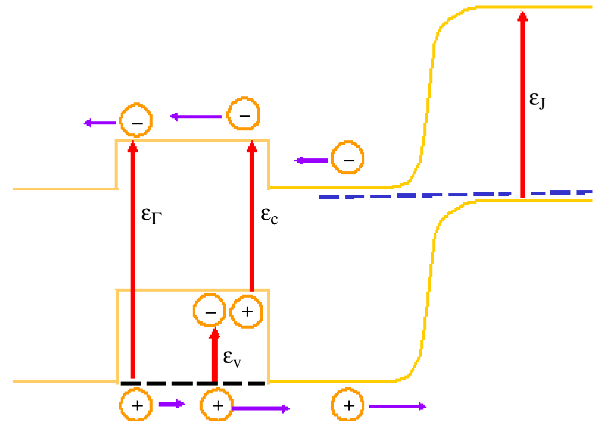

Figure 1. A simplified energy band diagram of the type II QD IB SCs.

there has been little work done on integration of type II QDs with the IB SCs.

Figure 1 displays the simplified energy band structure of the type II QD IB SCs. Unlike the conventional QD IB SCs [10, 11], the stack of QD layers of type II QD IB SCs is shown as not being sandwiched by the p- and n-doped layers. First, QDs are embedded far from the depletion layer and the built-in electric field, though at a distance less than the carrier diffusion length. Second, QDs have the type II energy band alignment that creates potential barriers for majority carriers and potential wells for minority carriers.

In this paper we report on the energy conversion in type II QD IB SCs. The mathematical model is developed in section 2. It is shown that the increase of the sunlight concentration leads to the rise of the potential barrier around QDs. The raised barrier suppresses the recombination activity in QDs. The two-photon absorption in QDs increases rapidly and dominates over recombination along with the increase in the sunlight concentration. We have revealed that the photocurrent and the conversion efficiency may be higher than in the conventional SCs. The potential of the Ge/Si system for fabricating type II QD IB SCs is analyzed in section 3. The assumed device structure is shown in section 4. Discussions are presented in section 5.

2. Model

2.1. Electron transitions in QDs

The simplified energy-band diagram of the type-II QD SCs in thermal equilibrium is shown in figure 1. The p–n junction and the stack of QD layers sandwiched by n-doped spacers are seen to be connected in series. QDs have the type II energy band alignment with potential barriers in the conduction band and potential wells in the valence band. QDs are embedded in the n-doped base of the p–n junction, far from the depletion layer and the built-in electric field, but at a distance less than the carrier diffusion length. A detailed balance exists among generation and recombination processes. The Fermi energy lies at the same value for all bands and states. QDs are uncharged since electronic states of the type II QDs are empty in the conduction band and full in the valence band.

We assume the concentrated sunlight is absorbed in QDs only. The photovoltage is induced by the electron–hole pairs generated in the stack and injected from the stack into the p–n junction.

The concentrated sunlight destroys the detailed balance and it induces additional electron transitions from the confined states into the conduction band and brings p_D holes into the confined states. The destroyed balance splits the Fermi level into the quasi-Fermi levels of (a) the conduction band, (b) the valence continuum band and (c) the confined states [1, 10]. The additional electron transitions also take away a negative charge of ep_D/N_D from the QDs, where N_D is the volume density of the QDs. Along with the removing of the charge, the potential barrier ε_L arises in the valence band around the QDs [16]. The induced barrier blocks any transfer of mobile holes back from the semiconductor into the charged QDs. Simultaneously the potential barrier in the conduction band blocks the transfer of mobile electrons into the QDs. The equation of continuity governs separation of the quasi-Fermi levels by the induced occupation of the confined states.

Under the ideal IB SC conditions [1], the balance of transitions, $G/N_D = j_C - j_{RC} = j_V - j_{RV}$, and the equation of continuity, $j_C + j_{RV} = j_V + j_{RC}$, in QDs reduce to equations (6) and (7) in [1], respectively. The transitions j_C, j_V, j_{RV} and j_{RC} must be calculated by equation (5) in [1]. Here j_C and j_V are the irradiation-induced electron transitions going from the confined electronic state into the conduction band and from the valence band into the confined electronic state in the QD; j_{RV} and j_{RC} are the recombination-induced transitions into the confined state from the valence continuum band and the conduction band, respectively.

In order to take into account the nonradiative transitions, we rewrite the transitions per QD [8, 9] as

$$j_C = \alpha_C g_C S_X/N_D \tag{1}$$

$$j_V = \alpha_V g_V S_X/N_D \tag{2}$$

$$j_{RV} = \alpha_V(g_V + g_{\Gamma V})S_X/[N_D + (\tau_V D_V N_V/\Omega N_{DV} L^2) \times \exp(\varepsilon_L/kT)] \tag{3}$$

$$j_{RC} = p_D/N_D\tau_C. \tag{4}$$

Here τ_C is the inter-band recombination lifetime for the electron transitions from the conduction band in the spacer into the confined state in QDs; τ_V is the intra-band relaxation lifetime for the electron transitions from the confined state into the valence continuum band within QDs; both τ_C and τ_V lifetimes include all radiative and nonradiative (including interface) mechanisms of transitions; S_X is the concentration of the sunlight; N_D is the volume density of the QDs; g_C, g_V and g_Γ are the integral intensities of infrared photons in the $\varepsilon_\Gamma < \hbar\omega < \varepsilon_\Gamma + \varepsilon_V$, $\varepsilon_V < \hbar\omega < \varepsilon_\Gamma$ and $\varepsilon_\Gamma + \varepsilon_V < \hbar\omega$ ranges of the solar spectrum, respectively; ε_Γ is the bandgap between the ground confined state and the Γ valley in the conduction band of QDs; ε_V is the bandgap between the ground confined state and the Γ valley in the valence continuum band of QDs; Ω is the volume of the QD; N_V is the density of electronic states in the valence band in the spacer; N_{DV} is the density of states in the valence continuum band in QDs; D_V is the diffusion coefficient of holes in the spacer; L is the distance from QDs to the depletion layer; α_C and α_V are the absorption coefficients for the direct optical transitions in QDs from the confined state into the conduction band and from the continuous valence band into the confined state, respectively. We assume $\alpha_V = \beta_V p_D$ and $\alpha_C = \beta_C(N_D\vartheta - p_D)$ where β_C and β_V are the relevant absorption cross sections; ϑ is the number of the confined states per QD involved in the absorption. Equation (3) is derived under the condition that QDs have more electrons in the confined state than holes in the valence continuum band; $(N_D\vartheta - p_D)/N_D > p_V\Omega(N_{DV}/N_V)\exp(-\varepsilon_L/kT)$, where p_V is the density of holes in the roughly $1/\alpha_V$-thick stack of QD layers:

$$p_V \approx \alpha_V(g_V + g_\Gamma)S_X(L^2/D_V)/[1 + (\Omega N_D N_{DV} L^2/\tau_V D_V N_V)\exp(-\varepsilon_L/kT)]. \tag{5}$$

Substituting the photo-induced barrier $\varepsilon_L = e^2 p_D/\varepsilon R N_D$ and the transitions j_C, j_V, j_{RV} and j_{RC} into the equation of continuity yields

$$p_D = \vartheta N_D\left[1 + \frac{1}{\tau_C g_C \beta_C S_X} + \frac{\beta_V g_V}{\beta_C g_C} - \frac{\beta_V(g_V + g_\Gamma)}{\beta_C g_C} \times \frac{\Omega N_D N_{DV} L^2}{\tau_V D_V N_V} \times \exp\left(-\frac{e^2}{\varepsilon k T R}\frac{p_D}{N_D}\right)\right]^{-1} \tag{6}$$

$$G = \left[1 - \frac{g_V + g_\Gamma}{g_V} \times \frac{\Omega N_D N_{DV} L^2}{\tau_V D_V N_V} \times \exp\left(-\frac{e^2}{\varepsilon k T R}\frac{p_D}{N_D}\right)\right] \times S_X \alpha_V g_V \tag{7}$$

where ε is the dielectric constant of the spacer and R is the height of the QD.

2.2. Photocurrent

For simplicity, we assume a weak surface recombination in the type II QD IB SCs. Then approximately all mobile carriers generated in the stack of QDs must be collected by the p–n junctions. The generated photocurrent can be calculated by integrating the two-photon transitions G and adding the result to the photocurrent $eS_X g_\Gamma(0)$ induced by conventional one-photon transitions, $eS_X g_\Gamma(0) + e\int G(z)\,dz$. We can simplify the integration by substituting $\partial g_V/\partial z = -\alpha_V g_V$ in the integral and $g_\Gamma(0)/g_V(0)$ for g_Γ/g_V in equation (7). Calculations reduce the total photocurrent j generated in the type II QD IB SCs to

$$j = eS_X g_V(0) \times \left[1 - \frac{g_V(d)}{g_V(0)}\right] \times \left[1 + \frac{g_\Gamma(0)}{g_V(0)}\right] \times \left[1 + \frac{\Omega N_D N_{DV} L^2}{\tau_V D_V N_V} \times \exp\left(-\frac{e^2}{\varepsilon k T R}\frac{p_D}{N_D}\right)\right]^{-1} \tag{8}$$

where d is the thickness of the stack.

2.3. Dark current

The stack of QD layers and the p–n junction are connected in series in the type II QD IB SC. In this circuit, the stack of QDs operates as a pump engine injecting electron–hole pairs into the p–n junction while the p–n junction generates the photovoltage and the photocurrent. Since the junction and the stack are separated in the space, one can expect that the dark current of the type II QD IB SCs is induced by the p–n junction only. In fact, the stack embedded at a distance less than the carrier diffusion length may have some contribution to the dark current. To evaluate this contribution to the dark current, we call the detailed balance arguments firstly [1].

According to equation (6) from [1] under the condition (7) from [1], the dark current $j_{\rm DK}$ can be written as $j_{\rm DK} = j_{\rm DJ} + j_{\rm DV}$ under the condition $j_{\rm DC} = j_{\rm DV}$, where $j_{\rm DC}$ and $j_{\rm DV}$ are the dark components of the electron transitions from the confined state into the conduction band and from the valence band into the confined states in QDs, and $j_{\rm DJ}$ is the dark current of the ideal p–n junction. Using equation (5) from [1], these currents can be expressed as $j_{\rm DJ} \approx (2kT\varepsilon_J^2/h^3c^2) \times \exp[-\varepsilon_J/kT]\exp(V/kT)$ and $j_{\rm DV} = j_{\rm DC} \approx (2kT\varepsilon_{\rm C}\varepsilon_{\rm V}/h^3c^2) \times \exp[-(\varepsilon_{\rm V}+\varepsilon_{\rm C}+V)/2kT]\exp(V/kT)$. The ratio of the currents, $j_{\rm DJ}/j_{\rm DV}$, gives the condition for omitting the contribution of QDs to the dark current in the type II QD IB SCs on the basis of the detailed balance arguments

$$\exp[(\varepsilon_{\rm V}+\varepsilon_{\rm C}-2\varepsilon_J+V)/2kT] > \varepsilon_{\rm C}\varepsilon_{\rm V}/\varepsilon_J^2. \qquad (9)$$

For taking into account the nonradiative transitions, we assume that the distance from QDs to the depletion layer is large enough to prevent tunneling of confined carriers from QDs into the depletion layer. Then the dark current in the p–n junction is dominated either by electron (hole) diffusion over the potential barrier in the depletion layer, $j_{\rm DDV} \simeq (D_{\rm V}/L)N_{\rm V} \times \exp[-(\varepsilon_J - V)/kT]$, or by the electron transitions involving both tunneling and recombination in the depletion layer. Evidently, if the contribution from QDs $j_{\rm RV}$ dominates in the total dark current, $j_{\rm RV} > j_{\rm DJ}$, it must also dominate over the diffusion component of the dark current, $j_{\rm RV} > j_{\rm DDV}$. Since the density of holes is $p_{\rm V} = N_{\rm V} \times \exp[-(\varepsilon_J - V)/kT]$ at the depletion layer, equations (3) and (5) can be used to rewrite the contribution of QDs to the dark current as $j_{\rm RV} \approx (\Omega N_{\rm D}N_{\rm DV}d/\tau_{\rm V}) \times \exp[-(\varepsilon_{\rm L}+\varepsilon_J - V)/kT]$. The ratio $j_{\rm DDJ}/j_{\rm RV}$ gives the condition for omitting the contribution of both radiative and nonradiative transitions in QDs to the dark current in the type II QD IB SCs:

$$\exp[\varepsilon_{\rm L}/kT] > \Omega N_{\rm D}N_{\rm DV}Ld/N_{\rm V}D_{\rm V}\tau_{\rm V}. \qquad (10)$$

2.4. Photovoltage and conversion efficiency

Under the open-circuit condition, the bias $V_{\rm OC}$ is induced, creating the precise balance $j_{\rm DK}(V_{\rm OC}) = j$ between the generated photocurrent j and the set current $j_{\rm DK}(V_{\rm OC})$. Under the conditions (9) and (10), the contribution of QDs to the dark current is small. The set current $j_{\rm DK}(V_{\rm OC})$ is reduced to the dark current of the p–n junction $j_{\rm DJ}(V_{\rm OC})$. Therefore, the open-circuit voltage $V_{\rm OC}$ induced in the type II QD IB SC will be approximately the same as that $V_{\rm OCO}$ induced in the conventional SC, $V_{\rm OC} = V_{\rm OCO} + nkT \times \ln(j/j_{\rm O})$, if both devices have the same quality p–n junctions with the same parameters like dark currents, ideality factors n and fill factors FF. On the other hand, the conversion efficiency of the type II QD IB SC η will increase, $\eta = \eta_{\rm O} \times (j/j_{\rm O})$. Here $\eta_{\rm O}$ and $j_{\rm O}$ are the conversion efficiency and the photocurrent generated in the conventional SC, $j_{\rm O} = eS_{\rm X}g_{\rm O}(0)$; $g_{\rm O}$ is the integral intensity of solar photons in the absorption spectrum of the conventional SC, $\varepsilon_{\rm O} < \hbar\omega$. Substituting j from equation (9) and $j_{\rm O}$ in η yields

$$\eta = \eta_{\rm O}\frac{g_{\rm V}(0)+g_\Gamma(0)}{g_{\rm O}(0)}\left[1-\frac{g_{\rm V}(d)}{g_{\rm V}(0)}\right] \times\left[1+\frac{\Omega N_{\rm D}N_{\rm DV}L^2}{\tau_{\rm V}D_{\rm V}N_{\rm V}}\times\exp\left(-\frac{e^2}{\varepsilon kTR}\frac{p_{\rm D}}{N_{\rm D}}\right)\right]^{-1}. \qquad (11)$$

2.5. The Auger limit

Under the concentrated light irradiation, the Auger recombination provides an intrinsic constraint upon the recombination lifetime, the open-circuit voltage and the efficiency of conventional Si SCs [17]. For the electron–hole recombination in the spacer between QDs in the stack of QD layers in the type II QD IB SCs, the Auger limit can be written as $\tau_{\rm A} = 1/C_{\rm A}p_{\rm V}^2 > L^2/D_{\rm V}$, where $\tau_{\rm A}$ and $C_{\rm A}$ are the Auger recombination lifetime and the Auger coefficient, respectively. Substituting $p_{\rm V}$ from equation (5) in $\tau_{\rm A}$ reduces the Auger limit to

$$S_{\rm X}(g_{\rm V}+g_\Gamma)\alpha_\Gamma L^3\sqrt{C_{\rm A}/D_{\rm V}^3} < 1. \qquad (12)$$

2.6. Recombination limits

While the recombination transitions balance the irradiation-induced electron transitions, the net generation G and the separation between the quasi-Fermi levels are very small. However, these parameters essentially increase as the irradiation-induced transitions become more intensive than the recombination transitions in QDs. After substituting $j_{\rm C}$, $j_{\rm RC}$, $j_{\rm V}$ and $j_{\rm RV}$ from equations (1) to (4) into $j_{\rm C} > j_{\rm RC}$ and $j_{\rm V} > j_{\rm RV}$, the following conditions can be found for the separation of the quasi-Fermi levels

$$\tau_{\rm C}g_{\rm C} > 1/S_{\rm X}\beta_{\rm C} \qquad (13)$$

$$g_{\rm V}\tau_{\rm V}\exp\left(\frac{e^2}{\varepsilon kTR}\frac{p_{\rm D}}{N_{\rm D}}\right) > \frac{g_\Gamma\Omega N_{\rm D}N_{\rm DV}L^2}{D_{\rm V}N_{\rm V}}. \qquad (14)$$

These conditions reduce equations (6), (7) and (11) to

$$p_{\rm D}(z) = \vartheta N_{\rm D}\beta_{\rm C}g_{\rm C}(z)/(\beta_{\rm C}g_{\rm C}(z)+\beta_{\rm V}g_{\rm V}(z)) \qquad (15)$$

$$G(z) = -S_{\rm X}\frac{\partial g_{\rm V}(z)}{\partial z} \qquad (16)$$

$$\frac{\eta-\eta_{\rm O}}{\eta_{\rm O}} = \frac{g_{\rm V}(0)+g_\Gamma(0)-g_{\rm O}(0)}{g_{\rm O}(0)}. \qquad (17)$$

2.7. Coordinate dependence

Equations $\partial g_{\rm C}/\partial z = -\alpha_{\rm C}(z)g_{\rm C}(z)$, $\partial g_{\rm V}/\partial z = -\alpha_{\rm V}(z)g_{\rm V}(z)$, $\alpha_{\rm C} = \beta_{\rm C}[N_{\rm D}\vartheta - p_{\rm D}(z)]$ and $\alpha_{\rm V} = \beta_{\rm V}p_{\rm D}(z)$ determine the integral intensities, $g_{\rm C}(z)$ and $g_{\rm V}(z)$, as a function of the distance z from the illuminated surface in the cell. If

$$g_{\rm C}(0) = g_{\rm V}(0) \qquad (18)$$

the conditions (13) and (14) reduce the integral intensities to $g_{\rm C}(z) = g_{\rm V}(z) = g_{\rm V}(0)\exp(-\alpha_{\rm V}z)$. Simultaneously, the dependence on z disappears in the confined state occupation, $p_{\rm D} = \vartheta N_{\rm D}\beta_{\rm C}/(\beta_{\rm C}+\beta_{\rm V})$, and in the absorption coefficients

$$\alpha_{\rm C} = \alpha_{\rm V} = \vartheta N_{\rm D}\beta_{\rm C}\beta_{\rm V}/(\beta_{\rm C}+\beta_{\rm V}). \qquad (19)$$

Since $g_{\rm V}(0) = (\varepsilon_\Gamma - \varepsilon_{\rm V})\gamma$ and $g_{\rm C}(0) = \varepsilon_{\rm V}\gamma$, where $\gamma \approx 2.5\times10^{17}$ cm^{-2} s^{-1} eV^{-1} is the density of photon flux in the solar spectrum in the range of 0.6 eV $< \hbar\omega <$ 1.5 eV [41], the condition (18) also yields

$$\varepsilon_\Gamma = 2\varepsilon_{\rm V}. \qquad (20)$$

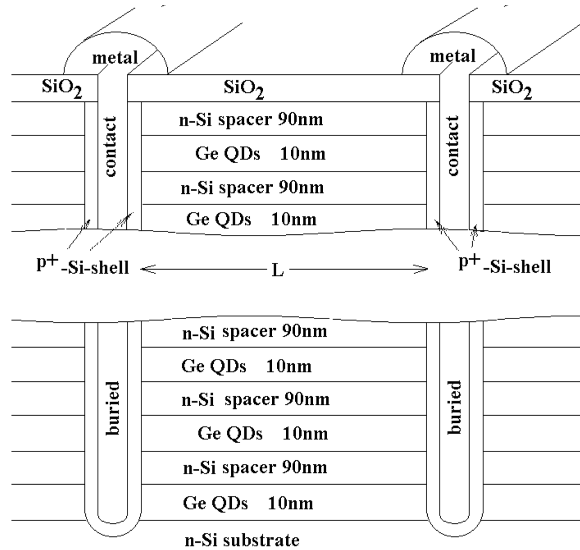

Figure 2. Schematic of the device structures.

3. Potential of Ge/Si system

3.1. Motivation

The choice of the Ge/Si material system for the type II QD IB SCs is motivated by its specific technological and photoelectrical properties. Ge and Si are indirect band semiconductors that offer very slow electron–hole recombination. The type II Ge QD has the real-space indirect fundamental bandgap at the interface with the Si matrix and the large discontinuity in the valence band. The band offset in the conduction band can grow up to 0.3 eV. The offset can be tuned by the strain at the interface, by the composition of the Si spacer and by the carbon-induced compensation of the strain [18, 19]. Experiments revealed large absorption cross sections in Ge QDs [20, 21]. The electron inter-band recombination lifetime is extended to 1 μs [14]. All of these data on Ge/Si material system are favorable for the type II QD IB SCs and offer the promise of achieving higher conversion efficiency devices. The compatibility with the Si-based integrated-circuit technologies gives the type II Ge QD IB Si SCs the advantage of having a lower cost for launching it into industrial production[5].

3.2. Technological aspect

These materials are completely miscible forming $Si_{1-x}Ge_x$ alloys with a gradually varying bandgap over the entire compositional range, from pure Si to pure Ge. Numerous studies have reported on the formation of the type II QD multilayer structures in Ge/Si system by MBE and MOCVD using the Stranski–Krastanow growth mode [20, 22–26]. A stack of $N_D = 2 \times 10^{16}$ cm^{-3} Ge QDs, similar to the stack shown in figure 2, has been grown recently [26]. The stack was composed of 50 QD layers with about 2×10^{11} cm^{-2} Ge QDs per layer. The 40 nm thick Si spacers separate the QD layers from each other [26].

A large interfacial strain induced by the 4% lattice mismatch between Ge and Si drives the growth of a strained Ge layer in the Stranski–Krastanow growth mode. The strained layer is converted into nanometer-sized Ge QDs to relax the strain when the deposited layer exceeds a critical thickness [20, 22, 24, 27]. The control over the strain is now successively used for tailoring energy bands in Ge/$Si_{1-x}Ge_x$ multilayer nanostructures [18, 28–32]. Composition of those QDs is also dependant on parameters of the Si spacer. For example, when the spacer is thinner than the critical thickness, the atomic inter-diffusion from the Si spacer into Ge QDs occurs to relax the residual strain further [20, 22, 28, 29]. The residual strain and the inter-diffusion may essentially modify both offset and profile of bandgaps at the Ge/Si interface [29]. The control over the composition may be used for tailoring the energy bands. An additional degree of freedom for tailoring both the band offsets and the strain in the Ge QDs can be provided by adding carbon [33]. Carbon has the smaller lattice constant and as experiments have shown it can completely compensate the strain at the Ge/Si interface [19, 34].

3.3. Conduction band alignment

3.3.1. Unstrained Ge. The lowest conduction band minima of unstrained Ge lie at the L points of symmetry in the $\langle 111 \rangle$ directions on the surface of the Brillouin zone. These minima constitute a 0.66 eV-wide indirect bandgap [35]. Another conduction band minimum lies in the Δ valleys in the $\langle 100 \rangle$ directions of the Brillouin zone. It constitutes a 0.85 eV-wide indirect bandgap. The Γ point of symmetry in the center of the Brillouin zone constitutes a 0.80 eV-wide direct band. The unstrained Ge/Si interface has the type-II band alignment with a 0.51 eV-wide offset in the valence band and a 0.05 eV-wide indirect band offset in the conduction band [35, 36].

3.3.2. Strained Ge/Si. Like the bulk samples, strained Si/Ge nanostructures have indirect fundamental bandgaps, ε_{Si} and ε_{Ge}, in Ge and Si layers. However, the residual interfacial strain essentially modifies both offsets and profile of the energy bands at the strained Ge/Si interface [14, 37]. The fundamental bandgap acquires the real-space indirect character at the interface [32, 37]. The real-space indirect bandgap dramatically reduces the oscillator strength of the radiative inter-band recombination at Ge QDs [38].

Both thermal expansion coefficient and lattice constant are larger in Ge than in Si. Usually a compressive strain is induced in Ge QDs while a tensile strain is induced in Si spacers [18, 28]. The energy band diagram of Si spacers with Ge QDs is shown in figure 3. The strain lifts the sixfold degeneracy of the conduction band in Δ valleys of the Brillouin zone and splits the Δ valleys into $\Delta 2$ and $\Delta 4$ valleys. The strain shifts these valleys in the opposite directions so that the $\Delta 2$ valley constitutes the conduction band minimum in the tensile strained Si spacer. The strain relaxing in the thick Si spacer may also lead to a confining potential of less than 25 meV for electrons in the conduction band of the Si at the Ge/Si interface [28, 29]. This small wrinkle drops to 0 at about 20 nm from the interface [28, 29]. The compressive

[5] The compatibility with Si-based integrated-circuit technologies is very important for investors. As a result, the production of silicon solar cells has increased since the 1990s and now composes 93% of all photovoltaic products despite strong competition from other promising photovoltaic materials.

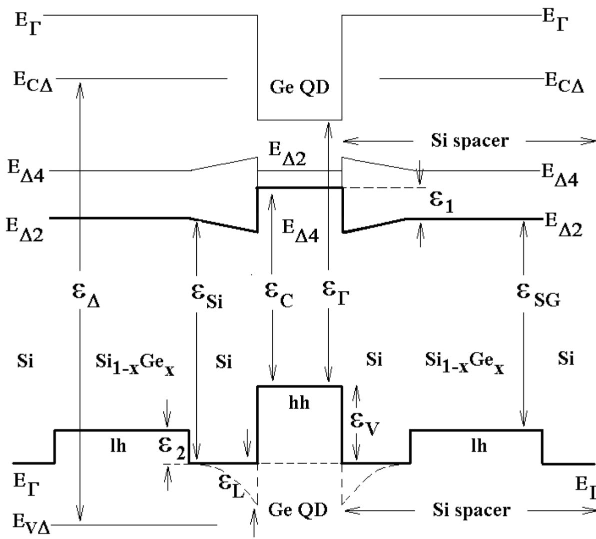

Figure 3. An energy band diagram of the multilayer absorber. ε_Δ is the energy gap for the direct optical transitions within the Si/$Si_{1-x}Ge_x$/Si spacer, from the Δ valence band ($E_{V\Delta}$) into the Δ conduction band ($E_{C\Delta}$), $\varepsilon_\Delta = E_{C\Delta} - E_{V\Delta}$; E_Γ is the energy of the Γ band in the conduction and valence bands; $E_{\Delta 2}$ and $E_{\Delta 4}$ are the energies of the split Δ bands in the conduction band; lh and hh are the light and the heavy holes.

strain pushes up the L valley and switches the conduction band minimum from the L valley to the $\Delta 4$ valley in Ge QDs [18, 28, 29]. The band offset in the conduction band, ε_1, increases up to 0.2 eV in the Δ valley [28, 30]. The band offset ε_1 can grow up to 0.3 eV in the type-II Ge/Si heterojunction, however, its growth is dependent on the strain and on the composition of the Si spacer and on the carbon-induced compensation of the strain in Ge QDs [18, 19].

The Γ point in the center of the Brillouin zone constitute a 3.4 eV-wide direct bandgap in Si and a 0.8 eV-wide direct bandgap in Ge [18]. Therefore, the potential energy profiles of the conduction and valence band edges in the Γ valleys exhibit the type-I alignment with the Γ band offset of about 2 eV in the conduction band at the Ge/Si interface. The potential energy profile over the interface also acquires the type-II alignment in the $\Delta 2$ valley: however, it may acquire the type-I alignment in the $\Delta 4$ valley [18, 28, 29]. The fundamental bandgap retains indirect in Ge QDs since under the strain the conduction band minimum at the $\Delta 4$ valley is lower than at the Γ valley.

3.4. Valence band alignment

The strain lifts the degeneracy between heavy and light holes at Γ valleys in the valence band. The heavy holes constitute the upper band edge in the compressively strained Ge QDs while the light holes constitute the upper band edge in the tensile strained Si spacer [18, 28, 29].

A confinement potential of the Ge QDs essentially modifies the energy band profile in the valence band. The confinement potential takes some electronic states from the valence continuum band edge at the Γ valley in the center of the Brillouin zone and confines them into Ge QDs. Instead the electronic states retained in the Γ valley constitute a new continuum band edge below the confinement potential in the valence band of the Ge QDs. The new band edge merges with the valence band edge at the QD/Si spacer interface. Simultaneously, the new continuum band edge constitutes a larger direct gap at the Γ point in the center of the Brillouin zone in the Ge QDs. As shown in figure 3, the confinement increases the direct bandgap in the Ge QDs by adding the valence band offset, $\varepsilon_V = 0.51$ eV, to the gap, $\varepsilon_\Gamma + \varepsilon_V$. The confinement also increases the direct ε_Γ and indirect ε_{Ge} bandgaps between the confined state and both the Γ and $\Delta 4$ valleys of the conduction band in the Ge QDs.

3.5. Absorption cross sections

The absorption cross section, β_Γ, can be roughly appraised from the absorption coefficient α_Γ and the effective number of oscillators $N_{C\Gamma}$ involved in the direct optical transitions between the Γ valleys, $\alpha_\Gamma \approx \beta_\Gamma N_{C\Gamma}$ [39]. Both α_Γ and $N_{C\Gamma}$ are proportional to $m_r^{3/2}$, where m_r is the reduced electron–hole mass $m_r = m_{e\Gamma} m_h/(m_{e\Gamma} + m_h)$. Electrons involved in the direct transitions between the Γ valleys in the bulk Ge essentially have a smaller mass than the involved holes, $m_{e\Gamma} = 0.041\ m_o$ and $m_h = 0.28\ m_o$ [40]. Therefore, the effective number of oscillators in the bulk Ge is approximately equal to the density of states in the Γ valley of the conduction band, $N_{C\Gamma} = 2 \times 10^{17}$ cm^{-3}. The effective cross section is about $\beta_\Gamma \approx 2.5 \times 10^{-14}$ cm^2.

A strong carrier confinement increases both oscillator strengths and absorption cross sections in QDs [3, 39]. Nevertheless, we will use the absorption cross sections of the bulk Ge, $\beta_\Gamma \approx 2.5 \times 10^{-14}$ cm^2, as a scale to appraise the absorption cross sections, β_C and β_V, in Ge QDs.

The absorption cross sections are also proportional to the dipole transition matrix elements $\langle \psi_F u_F | er | \psi_I u_I \rangle$, where $\psi_{F,I}(r)$ and $u_{F,I}(r)$ are the envelope function and the periodic Bloch function of the relevant final and initial wavefunctions (F and I, respectively) [39], e is the electronic charge, r is the electron space coordinate, and er is the electric dipole. This dipole matrix element is reduced to $\langle \psi_F | er | \psi_I \rangle$ for transitions between electronic states with the same Bloch function since $\langle u_V | er | u_V \rangle = 0$, e.g. for transitions in the same band (the intra-band transitions). On the other hand, the matrix element is reduced to $\langle u_C | er | u_V \rangle \langle \psi_C | \psi_V \rangle$ for transition between electronic states of different bands (the inter-band transitions) since the Bloch functions of conduction and valence bands are orthogonal to each other [39]. Therefore, the type-I alignment of the Γ bands never affects the periodic Bloch functions and the matrix element $\langle u_C | er | u_V \rangle$ of the direct optical transitions from the confined state to the conduction band at the Γ valley in Ge QDs. Moreover, the type-I alignment of the Γ bands induces resonant electronic states in the Γ valley within Ge QDs. This makes the overlapping of the envelope functions $\langle \psi_C | \psi_V \rangle$ and the oscillator strength stronger. Therefore, the larger cross section β_C is expected in Ge QDs, $\beta_C > \beta_\Gamma$. For the same reason, the absorption cross section β_V for the intra-band absorption must be $\langle \psi_{VF} | er | \psi_{VI} \rangle / \langle u_C | er | u_V \rangle \langle \psi_C | \psi_V \rangle$ times stronger than β_Γ.

Measurements of the inter-band absorption coefficient performed in the waveguide geometry for Ge QDs buried in the Si matrix revealed 10^3 cm^{-1} per 23 nm thick layer [21].

The absorption cross section of $\vartheta\beta_C \approx 8 \times 10^{-13}$ cm^2 per QD can be deduced from these experiments. The result is 30 times larger than $\beta_\Gamma = 2.5 \times 10^{-14}$ cm^2. A photoinduced spectroscopy technique used to measure the intra-band absorption cross section $\vartheta\beta_V$ per QD in Ge QDs buried in Si has revealed the experimental value of $\vartheta\beta_V = 2 \times 10^{-13}$ cm^2 [20]. This result is about ten times stronger than β_Γ. The discrepancy between estimated β_Γ and the measured values of the absorption cross sections per QD, $\vartheta\beta_C$ and $\vartheta\beta_V$, demonstrate that about $\vartheta = 10$ confined states per QD are effectively involved in the absorption in the Ge QDs. Then, $\beta_C = 3 \times 10^{-14}$ cm^2 and $\beta_V = 2 \times 10^{-14}$ cm^2 are realistic values reflecting the large measured values of the absorption cross sections in Ge QDs.

4. Device structure

In the type II QD IB SC applications it is crucial to maintain relatively high carrier mobility. The electrons and the holes generated in the stack of QD layers should be able to travel to the p–n junction before they recombine. Recent experiments have shown that the mobility in the stack of Ge/Si QD layers mainly depends on the structural and morphological properties of QDs [23]. Evidently, the mobility in the layered structure must be higher in the plane direction.

The buried contact approach provides an effective way of in-plane collecting the photogenerated carriers from the stack of QD layers. This approach also provides an additional performance improvement, a reduced shading loss arising from the top contact metal [41]. The assumed buried-contact structure of the type-II QD IB SC is shown in figure 2. The cell looks similar to the buried-contact conventional Si SC [41]. The stack of the type-II Ge QDs embedded in the n-doped Si is grown on the n-doped Si-wafer. The Si layers in the stack act as the spacers between the approximately 3 nm thick Ge QD layers. About 50 layers of these spacers make up an approximately 5 μm thick n-doped multilayer absorber with the silicon oxide layer covering this absorber. The oxide serves as a top surface passivation coating, reducing surface recombination rate along the solar cell surface. The p–n junctions of the type-II QD IB SC shown in figure 2 are formed with the p-doped shells buried deep in the grooves incorporated into the n-doped absorber. The processing developed for the buried-contact solar cells [41] can be also used for putting the p-doped shells into the graves in the n-doped QD absorber. For example, first, a laser can be used to cut grooves through the top silicon oxide layer and the underlying multilayer absorber; second, boron deposition and diffusion can be used to form p-doped shells around the grooves in the absorber; third, the electrodeless plating can be used selectively to deposit a metal contact on the p-doped conducting shell in the grooves. Like the buried p–n junctions of the buried-contact solar cells [41], these p–n junctions collect holes generated in the n-doped absorber in the type-II Ge QD buried Si solar cell.

The spacer can also have a more complex structure. In particular, the spacer shown in figure 4 is a three-layer heterostructure. The 50 nm thick n-doped $Si_{1-x}Ge_x$ alloy layer is built in between the two 20 nm thick n-doped Si barrier layers in this spacer. The spacer can serve as an in-plane channel collecting mobile holes. The amount of Ge

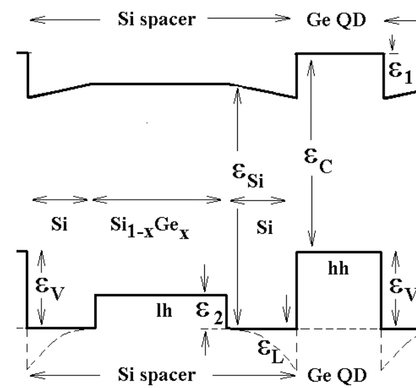

Figure 4. An energy band diagram of the three-layer heterojunction $Si/Si_{1-x}Ge_x/Si$ spacer.

in the $Si_{1-x}Ge_x$ alloy layer, $x < 0.2$, determines the energy band offset and the height of the barrier ε_2 at the $Si/Si_{1-x}Ge_x$ interface in the three-layer spacer. A small amount of Ge, $x \neq 0$, lets the Si layers in the $Si/Si_{1-x}Ge_x/Si$ spacer to act as the wide-band shell barrier around Ge QDs.

5. Results and discussions

5.1. Potential barriers

According to equations (6)–(11) and (13) and (14), the potential barriers around QDs are extremely important for the type II QD IB SCs performance. The potential barrier ε_1 separates mobile electrons from QDs in the conduction band while the potential barrier $\varepsilon_L + \varepsilon_2$ separate mobile holes from QDs in the valence band. Both separations occur in a real space; therefore, mobile electrons and holes recombine very seldom with confined electrons and holes.

The band offset in the conduction band, ε_1, depends on technological parameters like the strain, the composition of the Si spacer and the carbon-induced compensation of the strain in Ge QDs. The value of $\varepsilon_1 = 0.2$ eV was reported for the offset in the Δ valley [28, 30], however, the offset can grow up to 0.3 eV [18, 19].

The barrier ε_2 is created by heterojunctions in the complex three-layer spacers while the barrier ε_L is induced by sunlight illumination. Evidently, the stack with a simple one-layer Si spacer has an application advantage and, due to its importance here, we discuss the case of the one-layer spacers only, $\varepsilon_2 = 0$.

The Ge QDs buried in n-doped Si have a dense quasi-continuous energy spectrum of the confined states [42, 43]. About 55 confined states per QD were estimated from the capacitance measurements [43]. While the irradiation-induced barrier ε_L is small, the irradiation-induced mobile holes drop very fast from n-doped Si spacer into the Ge QDs. These holes relax very fast through the dense quasi-continuum of confined states into the ground confined state. The dropped holes fill the QDs very fast with positive charge. The accumulation (electron–hole inter-band recombination) time is long in the indirect bandgap semiconductors like Si and Ge [42]. Therefore, the accumulated charge can be large even at moderate excitation powers. The accumulated positive charge of the p_D confined holes induces the potential barrier

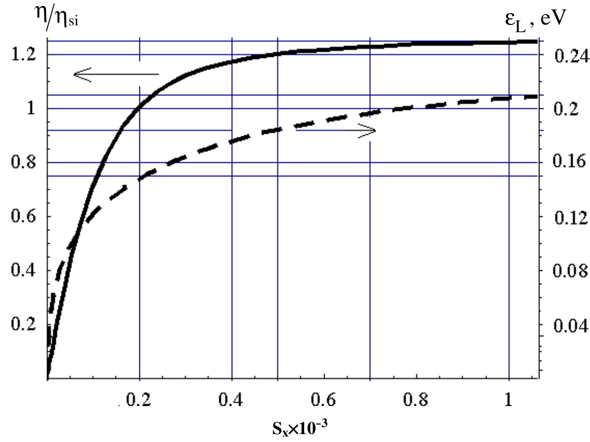

Figure 5. Conversion efficiency $\eta/\eta_{\rm Si} \approx j/j_{\rm Si}$ (solid line) and irradiation-induced barrier $\varepsilon_{\rm L}$ (dashed line) as a function of the concentration S_x.

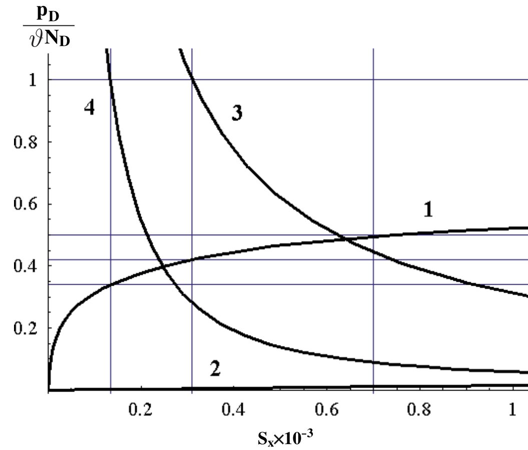

Figure 6. Irradiation-induced filling of the confined states with holes $p_{\rm D}/\vartheta N_{\rm D}$ and conditions in equations (12)–(14) as a function of the concentration S_x : 1—$p_{\rm D}/\vartheta N_{\rm D}$; 2—equation (12); 3—equation (13); 4—equation (14).

of $\varepsilon_{\rm L} = e^2 p_{\rm D}/\varepsilon R N_{\rm D}$ in the valence band. This barrier arising around the Ge QDs blocks diffusion of mobile holes from the Si spacer into the charged Ge QDs. The calculation shows that the potential $\varepsilon_{\rm L}$ grows about $e^2/\varepsilon R = 40$ meV per confined hole in Ge QDs that $\varepsilon = 11.9$ and $R = 3$ nm. In fact $e^2/\varepsilon R$ is the confined exciton binding energy, i.e. the energy gain that the mobile electron and the confined hole have due to attracting each other in the Ge QDs. The barrier ε_1 in the conduction band separates electron and hole in a real space and disallows them to screen each other in the QDs. Therefore, the potential appears around the QDs. Noteworthy, the exciton binding energy extracted from experiments on carrier transports through a photoexcited Ge QD system was also 40 meV [44].

Obviously, the irradiation-induced barrier $\varepsilon_{\rm L}$ can grow up from 0 to ε_1 but no more. Otherwise the mobile electrons begin to overwhelm the barrier ε_1 and screen the holes confined in the Ge QDs. Substituting $p_{\rm D}$ from equation (6) into $\varepsilon_{\rm L} = e^2 p_{\rm D}/\varepsilon R N_{\rm D}$, one can calculate the irradiation-induced barrier $\varepsilon_{\rm L}$ as a function of the sunlight concentration S_x. The following numerical values involving experimental data for parameters have been used in the calculations: $\varepsilon_1 = 0.2$ eV [28, 30], $kT = 26$ meV, $e^2/\varepsilon R = 40$ meV [44], $N_{\rm D} = 2 \times 10^{16}$ cm^{-3} [26], $N_{\rm V} \approx 2N_{\rm DV}$, $\vartheta = 10$, $\tau_{\rm V} = 50$ ps [16], $\tau_{\rm C} = 1$ μs [14], $L = 10$ μm, $g_{\rm C} = g_{\rm V} = 1.05 \times 10^{17}$ cm^{-2} s^{-1} [36], $g_\Gamma = 1.95 \times 10^{17}$ cm^{-2} s^{-1} [36], $\beta_{\rm C} = 3 \times 10^{-14}$ cm^2, $\beta_{\rm V} = 2 \times 10^{-14}$ cm^2, $\Omega = 10^3$ nm^3 [14, 26], $D_{\rm V} = 10$ cm^2 s^{-1}. The graph shown in figure 5 reveals that this irradiation-induced barrier can be as large as 0.18 eV at the concentration of $S_x = 400$ suns and as large as 0.2 eV at the concentration of $S_x = 700$ suns. It is noteworthy that the irradiation-induced large barrier around Ge QDs, $\varepsilon_{\rm L} \approx 0.17$ eV, was also extracted from experiments [16].

5.2. Imposed limits

5.2.1. Equation (20). The band offsets at the Ge/Si interface determine the two-photon absorption spectra in the type II QD IB SCs. It is crucial to maintain relatively high two-photon generation of mobile electrons and holes. Therefore, the band offsets should be adjusted to yield the effective absorption and generation by tuning parameters like the strain at the Ge/Si interface, the composition of the Si spacer and the carbon-induced compensation of the strain [18, 19]. According to equation (20) the most effective two-photon absorption occurs when $\varepsilon_\Gamma = 2\varepsilon_{\rm V}$. As reported in [40], the direct bandgap between the confined state and the Γ valleys in the Ge QD is $\varepsilon_\Gamma = 0.87$ eV. This yields $\varepsilon_{\rm V} = 0.43$ eV for the offset in the valence band. The same value is the energy gap between the valence continuous band and the confined state in the type II Ge QD IB Si SCs. The band offset at the QD Ge/Si interface is 0.25 eV in the conduction band between the $\Delta 2$ valley of the Si spacer and the Γ valley of the Ge QD.

5.2.2. Equation (13). Equation (13) gives the condition for separation of the quasi-Fermi level of the confined states from that in the conduction band. The separation depends on the inter-band recombination lifetime, $\tau_{\rm C}$. This lifetime includes both radiative and nonradiative (including interface) mechanisms of the electron transitions from the conduction band in the Si spacer into the confined state in the Ge QD. Equation (13) shows that the separation depends on the type-II band alignment of QDs via the barrier ε_1 as a parameter. This barrier creates the indirect real-space separation of the carriers that prevents the conduction band electrons from the fast recombination with the confined holes [14, 15]. As long as $\tau_{\rm C} \approx 1$ μs inter-band recombination lifetime has been extracted from experiments on the type-II Ge QDs buried in the Si [14] and the type-II GaSb QDs buried in the GaAs [15]. The inter-band recombination in the Si spacer has been estimated about 1 μs [14]. It is not clear yet how the real-space indirect-band separation in the conduction band suppresses inter-band recombination of mobile electrons with confined holes in the type-II QDs. Nevertheless, the suppression makes possible to liberate the quasi-Fermi level of the confined holes from that of the mobile electrons.

Equations (6) and (13) as a function of the sunlight concentration S_x are displayed in figure 6. Calculations have been made by substituting parameters into equations (6)

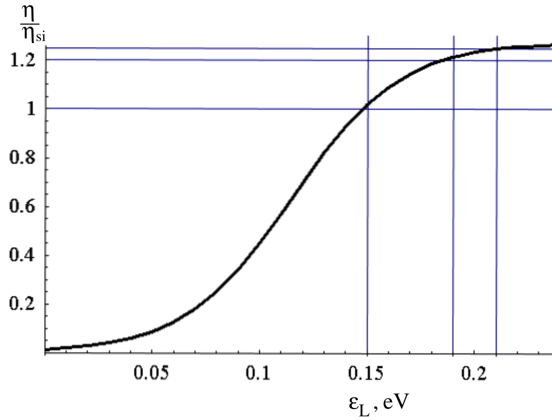

Figure 7. Conversion efficiency η/η_{Si} as a function of the barrier height ε_{L}.

and (13) for the numerical values given in section 5.1. The separation of the quasi-Fermi levels is seen to be at the concentration of $S_x = 300$. Under this concentration, the 42% of the confined states relevant to the absorption in the QDs, ϑ, are filled with holes.

5.2.3. Equation (14). Equation (14) gives the condition for separation of the quasi-Fermi level of the confined states from that of the continuum valence band. The separation depends on the intra-band recombination lifetime, τ_{V}. This lifetime includes both radiative and nonradiative transitions of electrons from the confined state into the valence continuum band in the Ge QDs. Equation (14) show that the separation depends on the irradiation-induced barrier ε_{L}. This barrier prevents mobile holes from dropping into the confined state inside the QDs. Moreover, the barrier supports diffusion of mobile holes in the plane of the Si spacer. Mobile holes must diffuse the distance L along the spacers to get the p–n junction in the type II Ge QD IB Si SCs. The mid-IR pump–probe experiments on Ge QDs buried in Si revealed $\tau_{\mathrm{V}} = 50$ ps-long intra-band relaxation lifetime [16]. The 'phonon bottleneck' effect and the acoustic phonon emission were suggested to be responsible for so much long intra-band relaxation lifetime [16].

Equations (6) and (14) as a function of the sunlight concentration S_x are displayed in figure 6. Calculations have been made by substituting parameters in equations (6) and (14) for the numerical values given in section 5.1. The separation of the quasi-Fermi levels is seen to be at the concentration of $S_x = 130$. Under this concentration, the 34% of the confined states relevant to the absorption in the QDs, ϑ, are filled with holes.

It is noteworthy that the conditions (13) and (14) are also relevant to the electronic states of recombination centers in doped and compound materials. For instance the abrupt decrease in the performance of GaInNAs solar cells by adding nitrogen, as noted in [13], indicates a fast relaxation of mobile electrons and an arrest of its quasi-Fermi levels by the nitrogen traps.

5.2.4. Equation (12). Equation (12) gives the Auger limit of the recombination lifetime in the type II Ge QD IB Si SCs. For the high conversion efficiency, the in-plane diffusion towards p–n junctions must be faster than the Auger recombination lifetime between the electrons and holes within the Si spacer layers. The Auger limit as a function of the sunlight concentration S_x is displayed in figure 6. Calculations have been made by substituting parameters in equation (12) for $C_{\mathrm{A}} = 10^{-31}$ cm^6 s^{-1} [17], $\alpha_\Gamma = 5 \times 10^3$ cm^{-1} and the numerical values given in section 5.1. The Auger recombination that is seen to be small must be omitted in the type II Ge QD IB Si SCs.

5.3. Dark current

5.3.1. Equation (9). Equation (9), $\exp[(\varepsilon_{\mathrm{V}} + \varepsilon_{\mathrm{C}} - 2\varepsilon_J + V)/2kT] > \varepsilon_{\mathrm{C}}\varepsilon_{\mathrm{V}}/\varepsilon_J^2$, where $2\varepsilon_J > \varepsilon_{\mathrm{V}} + \varepsilon_{\mathrm{C}} > \varepsilon_J > \varepsilon_{\mathrm{V}}, \varepsilon_{\mathrm{C}}$, evaluates the contribution of QDs into the dark current in the frame of the detailed balance arguments [1]. It is seen that this contribution dominates and the QDs operate as a fast recombination center until the bias $V < 2\varepsilon_J - \varepsilon_{\mathrm{V}} + \varepsilon_{\mathrm{C}}$. The contribution of the QDs into the dark current is reduced along with the biased increase. The contribution can be omitted from consideration at large biases, $V > 2\varepsilon_J - \varepsilon_{\mathrm{V}} + \varepsilon_{\mathrm{C}}$, e.g. under concentrated sunlight, when the large photovoltage is induced and the potential barrier appears around the QDs.

5.3.2. Equation (10). Equation (10), $\exp[\varepsilon_{\mathrm{L}}/kT] > \Omega N_{\mathrm{D}} N_{\mathrm{DV}} Ld/N_{\mathrm{V}} D_{\mathrm{V}} \tau_{\mathrm{V}}$, also evaluates the contribution of the QDs into the dark current of the type II QD IB SCs. However, this equation takes into account nonradiative transitions. Substituting the numerical values of parameters given in section 5.1 into the right-hand side of equation (10) yields $\Omega N_{\mathrm{D}} N_{\mathrm{DV}} Ld/N_{\mathrm{V}} D_{\mathrm{V}} \tau_{\mathrm{V}} \approx 10$. It is seen that this contribution dominates and the QDs operate as a fast recombination center until $\varepsilon_{\mathrm{L}} < 0.1$ eV. The contribution into the dark current reduces along with the irradiation-induced barrier as ε_{L} increases. Under the concentrated sunlight, when $\varepsilon_{\mathrm{L}} > 0.1$ eV, the contribution of the QDs to the dark current is small. Therefore, it can be omitted from consideration.

5.4. Photon flux

Photons from the $\varepsilon_\Gamma < \hbar\omega < \varepsilon_\Gamma + \varepsilon_{\mathrm{V}}$, $\varepsilon_{\mathrm{V}} < \hbar\omega < \varepsilon_\Gamma$ and $\varepsilon_\Gamma + \varepsilon_{\mathrm{V}} < \hbar\omega$ regions of the solar spectrum can induce the direct optical transitions in the Ge QDs in the type II Ge QD IB Si SCs. For simplicity, we assume that the sunlight is absorbed in the Ge QDs only. The direct bandgap is $\varepsilon_\Gamma = 0.87$ eV [40]. According to equation (20), under the condition (18), the offset in the valence band must be $\varepsilon_{\mathrm{V}} = 0.43$ eV. For these bandgaps, the integral intensities of irradiation are $g_{\mathrm{C}} = g_{\mathrm{V}} = 1.05 \times 10^{17}$ cm^{-2} s^{-1} and $g_\Gamma = 1.95 \times 10^{17}$ cm^{-2} s^{-1} [36].

5.5. Absorption coefficients

According to section 5.2.1, the confinement potential and the interfacial strain increases the direct energy bandgap between Γ valleys ε_Γ from 0.8 eV in the bulk Ge to $\varepsilon_\Gamma + \varepsilon_{\mathrm{V}} = 1.3$ eV in the Ge QDs [20, 40]. Photons with higher energy, 1.3 eV $< \hbar\omega$, directly transfer electrons from the valence continuum bands into the conduction band in the Ge QDs. Obviously, the absorption coefficient α_Γ for these direct optical transitions

between the Γ valleys must be as large as it is in the same quality bulk Ge, $\alpha_\Gamma \geqslant 5 \times 10^3$ cm^{-1}.

The confined states of the Ge QDs are at the Γ point of symmetry in the center of the Brillouin zone. Photons from both $\varepsilon_\Gamma < \hbar\omega < \varepsilon_\Gamma + \varepsilon_V$ and $\varepsilon_V < \hbar\omega < \varepsilon_\Gamma$ spectral regions, therefore, directly transfer electrons from the confined states into the Γ valley in the conduction band and from the Γ valley of the valence continuum band into the confined states, respectively. The two-photon transitions via these confined states are proportional to both illumination intensity and recombination lifetime. Either the intensity or the lifetime must be so large that, after the first-photon induced electron transition from the valence band into the confined state, this electron has a large probability for the second-photon induced transition from the confined state into the conduction band. Equations (13) and (14) show how large the product of the illumination intensity and the recombination lifetime must be for the illumination to induce the effective two-photon transitions. Evidently, the concentration of light S_X and the real-space separation of carriers support the net electron transitions in the QDs.

The equation of continuity sets the proper occupation p_D of the confined electronic state. The filling of the confined state with holes $p_D/\vartheta N_D$ as a function of the sunlight concentration S_x is displayed in figure 6. Calculations made by substituting the numerical values of parameters given in section (5.1) into equation (6). The occupation grows to $p_D/\vartheta N_D \approx 0.5$ at the concentration of $S_X \approx 700$ suns. The striking consequence of the type-II band alignment is the irradiation-induced barrier in the valence band around the QDs. Figure 5 shows that this barrier can be as high as $\varepsilon_L = 0.2$ eV at the concentration of $S_X \approx 700$ suns. Under the concentration of $S_x = 130$ suns, 34% of confined states relevant to the absorption in the QDs are filled with holes. The confined states are already very close to the optimal filling for the two-photon absorption. Substituting $N_D = 2 \times 10^{16}$ cm^{-3}, $\vartheta = 10$, $\beta_C = 3 \times 10^{-14}$ cm^2, and $\beta_V = 2 \times 10^{-14}$ cm^2 into equation (19) gives $\alpha_C = \alpha_V \approx 2.4 \times 10^3$ cm^{-1} for the two-photon absorption in the type II Ge QD IB Si SCs.

5.6. Photocurrent and conversion efficiency

In a few femtoseconds the irradiation-induced mobile electrons and holes slide from the 3 nm thick Ge QDs into the Si spacer. These electrons relax in the spacer in picoseconds, e.g. by emission of optical phonons. In particular, the electrons relax from the Γ valley into the Δ2 valley in the conduction band. The potential barriers around the Ge QDs, ε_1 and ε_L, separate mobile electrons and holes from the confined electronic states in a real space and suppress both the radiative and nonradiative transitions back into the QDs.

The equation of continuity sets the proper intensity G of the net transitions through the confined state. This equation also sets the proper injection of the mobile electron–hole pairs into the p–n junction in the type II Ge QD IB Si SCs. Equation (8) and figure 6 reveal an exponential dependence of the injection-induced photocurrent j on the barrier height in the valence band, $\varepsilon_L = e^2 p_D/\varepsilon R N_D$. The concentration S_X also impacts the photocurrent j and the conversion efficiency η of the type II Ge QD IB Si SCs via the induced barrier. The ratio $\eta/\eta_{Si} \approx j/j_{Si}$ is plotted as a function of the concentration S_X in figure 7. The numerical values of parameters are given in section 5.1. The conversion efficiency η of the type II Ge QD IB Si SCs is even seen to drop below the conversion efficiency η_{Si} of the conventional Si solar cells when the concentration $S_X < 200$ suns and $\varepsilon_L < 0.15$ eV since the conditions (13) and (14) are not met. At these concentrations, the QDs are seen to act as active recombination centers.

The conversion efficiency of the type II Ge QD IB Si SCs, η, however, grows fast with the concentration S_X. It already becomes $\eta = 1.2\ \eta_{Si}$ at the concentration of $S_X \approx 500$ that $\varepsilon_L \approx 0.184$ eV as shown in figure 5. The conversion efficiency of $\eta = 1.25\ \eta_{Si}$ is achieved at the concentration of $S_X \approx 1000$ suns such that $\varepsilon_L \approx 0.21$ eV. At this concentration, equations (8) and (10) give $j \approx 47.5$ A cm^{-2} for the photocurrent induced in the type II Ge QD IB Si SCs, and $j_{Si} \approx 38$ A cm^{-2} [36] for the photocurrent induced in the conventional Si solar cell. Assuming the same parameters like dark current, ideality factor n and fill factor FF for both devices, the enhanced photocurrent increases nearly 25% the conversion efficiency of the type II Ge QD IB Si SCs in comparison to the same quality conventional Si SC. In particular, the conversion efficiency limit calculated with the detailed balance arguments for the ideal one-p–n-junction Si SC will increase from 37% [36] to 46% in the type II Ge QD IB Si SCs.

6. Conclusion

In this work we have modeled the effect of the type II band alignment on the energy conversion in QD IB SCs. The important factor of this modeling is that increasing the sunlight concentration leads to suppressing the recombination activity in QDs. Simultaneously, the two-photon absorption rapidly increases in QDs. The contributions of QDs into the dark current in the type II QD IB SC is reduced and can be neglected. The photocurrent and the conversion efficiency may be higher than in the conventional SCs. The potential of Ge/Si system for fabrication of the type II QD IB SC has been analyzed. The main conclusion of this analyzes is that the type II Ge QD IB Si SCs will generate about 25% higher photocurrent and conversion efficiency than the same quality conventional Si SC.

Acknowledgments

We thank Daniel L Clinciu, and the referees for their comments. This work was supported by National Science Council of Taiwan under grant no. NSC 95-2112-M-009-046 and partly supported by Armenian Ministry of Education and Science under grant 0441-136-01.02.2005.

References

[1] Luque A and Marti A 1997 Increasing the efficiency of ideal solar cells by photon induced transitions at intermediate levels *Phys. Rev. Lett.* **78** 5014

[2] Sala G 2005 PV concentration in Spain: technology and market perspectives *Taiwan Symp. on HCPV Systems (INER, Taiwan, Nov. 2005)*

[3] Cuadra L, Martí A, Lopez N and Luque A 2004 Phonon bottleneck effect and photon absorption in self-ordered

quantum dot intermediate band solar cells *19th European Photovoltaic Solar Energy Conf. and Exhibition (Paris, June 2004)*

[4] Martí A, Cuadra L and Luque A 1999 Quantum dot super solar cell *Proc. Conf. on Sobre Dispositivos Electrónicos (Madrid)* pp 363–6

[5] Martí A, Cuadra L and Luque A 2000 Quantum dot intermediate band solar cell *Proc. 28th IEEE Photovoltaic Specialist Conf. (Fairbanks, AK, 2000)*

[6] Luque A and Martí A 2001 A metallic intermediate band high efficiency solar cell *Prog. Photovolt. Res. Appl.* **9** 73–86

[7] Nozik A J 2002 Quantum dot solar cells *Physica* E **14** 115

[8] Kechiantz A M, Sun K W, Kechiyants H M and Kocharyan L M 2005 Self-ordered Ge/Si quantum dot intermediate band photovoltaic solar cells *Int. Sci. J. Alternat. Energy Ecol.* **12** 85–7

[9] Kechiantz A M, Sun K W, Kechiyants H M and Kocharyan L M 2005 Suppression of dark current in two-step photovoltaic cells *Proc. 5th Int Conf. on Semiconductor Micro- and Nano-Electronics (Aghveran, Sept. 2005)* p 235

[10] Luque A, Marty A, Stanley C, Lopez N, Cuadra L, Zhou D, Pearson J L and McKee A 2004 General equivalent circuit for intermediate band devices: potentials, currents and electroluminescence *J. Appl. Phys.* **96** 903–8

[11] Luque A, Martí A, Lopez N, Antolín E, Cánovas E, Stanley C, Farmer C, Caballero L J, Cuadra L and Balenzategui J L 2005 Experimental analysis of the quasi-Fermi level split in quantum dot intermediate-band solar cells *Appl. Phys. Lett.* **87** 083505

[12] Nelson J, Ballard I, Barnham K, Connolly J P, Roberts J S and Pate M 1999 Effect of quantum well location on single quantum well p–i–n photodiode dark currents *J. Appl. Phys.* **86** 5898

[13] Kurtz S, Johnston S and Branz H M 2005 Capacitance-spectroscopy identification of a key defect in N-degraded GalnNAs solar cells *Appl. Phys. Lett.* **86** 113506

[14] Fukatsu S, Sunamura H, Shiraki Y and Komiyama S 1997 Phononless radiative recombination of indirect excitons in a Si/Ge type-II quantum dot *Appl. Phys. Lett.* **71** 258

[15] Hatami F *et al* 1998 Carrier dynamics in type-II GaSb/GaAs quantum dot *Phys. Rev.* B **57** 4635–41

[16] Halsall M P, Dunbar A D F, Shiraki Y, Miura M and Wells J-P R 2004 Hole confinement and dynamics in δ-doped Ge quantum dots *J. Lumin.* **108** 329–32

[17] Green M 1984 Limits on the open-circuit voltage and efficiency of silicon solar cells imposed by intrinsic Auger processes *IEEE Trans. Electron. Devices* **31** 611–8

[18] Schaffler F 1997 High-mobility Si and Ge structures *Semicond. Sci. Technol.* **12** 1515–49

[19] Schmidt O G and Eberl K 2000 Photoluminescence of monolayer to submonolayer thick $Ge_{1-z}C_z$ on Si(111) *Semicond. Sci. Technol.* **15** 399–402

[20] Boucaud P, Le Thanh V, Sauvage S, Debarre D and Bouchier D 1999 Intraband absorption in Ge/Si self-assembled quantum dots *Appl. Phys. Lett.* **74** 401–3

[21] Elkurdi M, Boucaud P, Sauvage S, Kermarrec O, Campidelli Y, Bensahel D, Saint-Girons G and Sagnes I 2002 Near-infrared waveguide photodetector with Ge'Si self-assembled quantum dots *Appl. Phys. Lett.* **80** 509–11

[22] Chang W-H, Chen W-Y, Chou A-T, Hsu T-M, Chen P-S, Pei Z and Lai L-S 2003 Effects of spacer thickness on optical properties of stacked Ge/Si quantum dots grown by chemical vapor deposition *J. Appl. Phys.* **93** 4999–5002

[23] Bao Y, Liu W L, Shamsa M, Alim K, Balandin A A and Liu J L 2005 Electrical and thermal conductivity of Ge/Si quantum dot superlattices *J. Electrochem. Soc.* **152** G432

[24] Schmidt O G and Eberl K 2000 Multiple layers of self-assembled Ge'Si islands: Photoluminescence, strain fields, material interdiffusion, and island formation *Phys. Rev.* B **61** 13721–9

[25] Tong S, Liu F, Khitun A, Wang K L and Liu J L 2004 Tunable normal incidence Ge quantum dot midinfrared detectors *Appl. Phys. Lett.* **96** 773–6

[26] Konle J, Presting H and Kibbel H 2003 Self-assembled Ge-islands for photovoltaic applications *Physica* E **16** 596

[27] Shchukin V A and Bimberg D 1999 Spontaneous ordering of nanostructures on crystal surfaces *Rev. Mod. Phys.* **71** 1125

[28] Schmidt O G, Eberl K and Rau Y 2000 Strain and band-edge alignment in single and multiple layers of self-assembled Ge/Si and GeSi/Si islands *Phys. Rev.* B **62** 16715–20

[29] El Kurdi M, Sauvage S, Fishman G and Boucaud P 2006 Band-edge alignment of SiGe/Si quantum wells and SiGe/Si self-assembled islands *Phys. Rev.* B **73** 195327

[30] Liu C W, Maikap S and Yu C-Y 2005 Mobility-enhancement technologies *IEEE Circuits Devices Mag.* **21** (May/June) 21–36

[31] Lee M L, Fitzgerald E A, Bulsara M T, Currie M T and Lochtefeld A 2005 Strained Si, SiGe, and Ge channels for high-mobility metal-oxide-semiconductor field-effect transistors *J. Appl. Phys.* **97** 011101

[32] Sfina N, Lazzari J-L, Derrien J, d'Avitaya F A and Said M 2005 Strain-balanced $Si_{1-x}Ge_x$/Si type II quantum wells for 1.55 μm detection and emission *Eur. Phys. J.* B **48** 151–6

[33] Galdin S, Dollfus P, Aubry-Fortuna V, Hesto P and Osten H J 2000 Band offset predictions for strained group IV alloys: $Si_{1-x-y}Ge_xC_y$ on Si(001) and $Si_{1-x}Ge_x$ on $Si_{1-z}Ge_z$ (001) *Semicond. Sci. Technol.* **15** 565–72

[34] Osten H J 1998 Band-gap changes and band offsets for ternary $Si_{1-x-y}Ge_xC_y$ alloys on Si(001) *J. Appl. Phys.* **84** 2716–21

[35] Taraschi G, Langdo T A, Currie M T, Fitzgerald E A and Antoniadis D A 2002 Relaxed SiGe-on-insulator fabricated via wafer bonding and etch back *J. Vac. Sci. Technol.* B **20** 725–7

[36] Sze S M 1981 *Physics of Semiconductor Devices* (New York: Wiley)

[37] Dashiell M W, Denker U and Schmidt O G 2001 Photoluminescence investigation of phononless radiative recombination and thermal-stability of germanium hut clusters on silicon(001) *Appl. Phys. Lett.* **79** 2261

[38] Laheld U E H, Pedersen F B and Hemmer P C 1995 Excitons in type-II quantum dots: finite offsets *Phys. Rev.* B **52** 2697

[39] Haug H and Koch S W 1993 *Quantum Theory of the Optical and Electronic Properties of Semiconductors* (Singapore: World Scientific)

[40] Kou Y-H, Lee Y K, Ge Y, Ren S, Roth J E, Kamins T I, Miller D A B and Harris J S 2005 Strong quantum-confined Stark effect in germanium quantum-well structures on silicon *Nature* **437** 1334–6

[41] Green M A 1998 *Solar Cells in Modern Semiconductor Device Physics* ed S M Sze (New York: Wiley)

[42] Boucaud P, Sauvage S, Elkurdi M, Mercier E, Brunhes T, Le Thanh V, Bouchier D, Kermarrec O, Campidelli Y and Bensahel D 2001 Optical recombination from excited states in Ge'Si self-assembled quantum dots *Phys. Rev.* B **64** 155310

[43] Kapteyn C M A, Lion M, Heitz R, Bimberg D, Miesner C, Asperger T, Brunner K and Abstreiter G 2000 Many-particle effects in Ge quantum dots investigated by time-resolved capacitance spectroscopy *Appl. Phys. Lett.* **77** 4169–71

[44] Li P W, Kuo D M T and Hsu Y C 2006 Photoexcitation effects on charge transports of Ge quantum-dot resonant tunneling diodes *Appl. Phys. Lett.* **89** 133105